

Cyclic Fatigue Behavior of Si_3N_4 Ceramics*

M. Masuda, T. Soma & M. Matsui

NGK Insulators Ltd, Nagoya, Japan

(Received 16 October 1989; revised version received 24 April 1990; accepted 4 May 1990)

Abstract

Tension–compression fatigue tests and alternating cantilever bending fatigue tests were carried out to clarify the fatigue behavior of sintered silicon nitride (Si_3N_4). Cyclic fatigue at room temperature depended mainly on the number of cycles accumulated rather than on time. An alternating load accelerated the fatigue process much more than a pulsating load. The modified Goodman line agreed well with the results of the fatigue test at room temperature. The design methodology proposed for metal fatigue would be applicable to the sintered Si_3N_4 used in this study. At high temperatures, however, the cyclic fatigue depended on frequency. At high temperatures, the lower the frequency, the less the fatigue resistance. A failure diagram was constructed to show effects of mean stress and stress amplitude on the fatigue strength. An equation expressing allowable stress under cyclic loading was proposed. Microstructural observations suggest that fatigue of sintered Si_3N_4 at room temperature is caused by microcracks at the grain boundaries. The progress of cyclic fatigue at high temperatures is caused by slow crack growth and creep deformation.

Um das Ermüdungsverhalten gesinterten Siliziumnitrids (Si_3N_4) besser zu verstehen, wurden Dauerschwingversuche im Zug–Druck Modus und mit wechselnder Biegebelastung an einseitig eingespannten Stäben durchgeführt. Das Ermüdungsverhalten bei Raumtemperatur hing hauptsächlich von der Anzahl der Lastwechsel, nicht aber von der Versuchsdauer ab. Wechselbelastung beschleunigte das Versagen viel mehr als Schwellbeanspruchung.

Die modifizierte Auswertung nach Goodman stimmte gut mit den bei Raumtemperatur erhaltenen Ergebnissen der Tests überein. Die Konstruktionsrichtlinien, die für die Ermüdung von Metallen vorgeschlagen wurden, wären für das in dieser Arbeit verwendete gesinterte Si_3N_4 anwendbar. Bei hohen Temperaturen zeigte sich jedoch eine Abhängigkeit des Ermüdungsverhaltens von der Frequenz der Lastwechsel. Je geringer die Frequenz bei hoher Temperatur ist, desto eher versagt das Material. Es wurde ein Ermüdungsdiagramm konstruiert, das den Einfluß der Mittelspannung und der Belastungsamplitude auf die Wechselfestigkeit wiedergibt. Ferner wurde eine Gleichung aufgestellt, die die Berechnung der zulässigen Belastung bei Dauerschwingbeanspruchung ermöglicht. Gefügeuntersuchungen deuten darauf hin, daß die Ermüdung gesinterten Si_3N_4 bei Raumtemperatur durch Mikrorisse an den Korngrenzen verursacht wird. Bei hohen Temperaturen wird die Ermüdung durch langsames Rißwachstum und durch Kriechverformung verursacht.

On a étudié le comportement en fatigue du nitrure de silicium (Si_3N_4) fritté par des essais de tension–compression ainsi que par des essais en flexion cantilever alternée. A température ambiante, le comportement en fatigue cyclique de ce matériau dépend plus du nombre de cycles accumulés que du temps. Une charge alternée accélère davantage le processus de fatigue qu'une charge pulsante. Ces résultats sont en bon accord avec ceux du concept de Goodman modifié. La méthode, proposée pour la fatigue des métaux peut ainsi être extrapolée au Si_3N_4 fritté utilisé lors de notre étude. A température élevée, le comportement en fatigue cyclique est dépendant de la fréquence: plus cette dernière sera basse et plus la résistance à la fatigue sera faible. On a élaboré un diagramme de rupture montrant l'influence de la contrainte moyenne

* Presented at the Symposium of Advanced Materials Science and Engineering Society, 16–17 March 1989, Tokyo, Japan.

et de l'amplitude de contrainte. On propose une équation donnant l'expression de la contrainte admissible sous charge cyclique. Les observations microstructurales suggèrent que la fatigue à température ambiante du Si_3N_4 fritté est causée par des microfissures situées aux joints de grains. L'évolution de la fatigue à haute température est due à la propagation lente des fissures et à une déformation en fluage.

1 Introduction

Various advanced ceramics are being studied for use as structural components such as gas turbine rotors,^{1,2} diesel engine components³ and bearing parts.⁴ Silicon nitride (Si_3N_4) is a leading candidate among those ceramics, because of its high mechanical strength and high heat resistance. To successfully design and utilize this material for mechanical components, the effect of cyclic loading on fatigue failure should be clarified.

Accelerated fatigue tests were made by the resonant bending method to accumulate fatigue data up to 10^{10} cycles for sintered Si_3N_4 , and to clarify the effects of frequency on cyclic fatigue at room temperature. To compare cyclic fatigue at room temperature and at high temperatures, tension-compression fatigue tests on sintered Si_3N_4 were also conducted. Two kinds of sintered Si_3N_4 (SSN-A and SSN-B) were studied. Mechanical properties of these materials are shown in Table 1. The sintering additives were: for SSN-A, SrO, MgO, CeO₂ and ZrO₂, and for SSN-B, Y₂O₃, MgO and ZrO₂, respectively. In the case of SSN-A, three different kinds of lot (SSN-A1 to A3) were used.

2 Cyclic Fatigue Behavior at Room Temperature

Figure 1⁵ shows the stress-number curve for tapered beam specimens of SSN-A2 under alternating load, at

Table 1. Mechanical properties of sintered Si_3N_4

Materials	Density (g/cm ³)	Four-point bending strength ^a (MPa)	Fracture toughness ^b (MN/m ^{3/2})	Young's modulus (GPa)
SSN-A1	3.21	740	6.2	265
SSN-A2	3.24	820	6.3	270
SSN-A3	3.28	860	6.2	275
SSN-B	3.25	970	6.1	300

^a According to JIS R1601.¹¹

^b Chevron notch method.

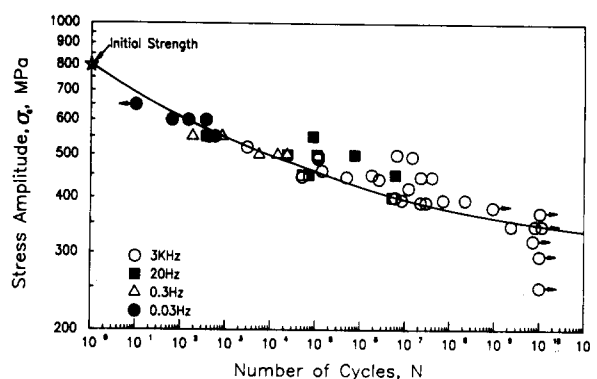


Fig. 1. S-N curve of cantilever beam specimens of SSN-A2 under alternating load, at frequencies from 0.03 Hz to 3 kHz.

frequencies from 0.03 Hz to 3 kHz. The use of high frequencies reduces the amount of time needed to test more than 10^{10} cycles. No heat was generated in the ceramic specimens under cyclic loading at a frequency of up to 3 kHz, unlike in the case of metals and polymers. Cyclic fatigue behavior of sintered Si_3N_4 appears to depend principally on the number of cycles rather than on time, because the fatigue strength at various frequencies did not show any discontinuities against the number of cycles. The solid curve suggests a decrease in the fatigue limit to about 40% of its initial strength.

Figure 2⁶ shows the mean stress/stress amplitude diagram of SSN-A1 at room temperature. σ_t on the horizontal axis represents the mean tensile strength of 6-mm diameter button-head specimens. Open circles represent specimens surviving at 10^7 cycles, and closed circles represent the failed specimens. The dotted line represents tensile strength. Alternating

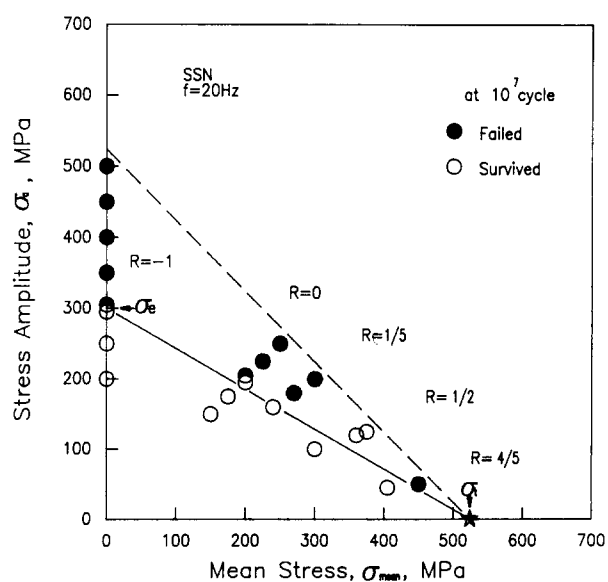


Fig. 2. Mean stress versus stress amplitude for fatigue failure in SSN-A1 at 10^7 cycles measured by high cycle fatigue test at room temperature. The solid line represents tensile strength.

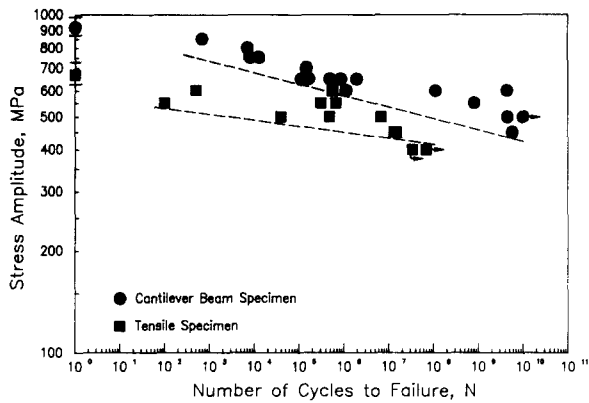


Fig. 3. The effect of volume on cyclic fatigue at room temperature. Cantilever beam specimens and the tensile specimens of SSN-B were used; the former have a small volume and the latter have a large volume.

load decreased strength to a larger extent than pulsating load. This diagram shows more clearly the safe stress state regions. The solid line from σ_e to σ_t represents a modified Goodman line,⁷ which is expressed by eqn (1) and is used as a design criterion for metal components:

$$\sigma_a = \sigma_e(1 - (\sigma_m/\sigma_t)) \quad (1)$$

where σ_a is stress amplitude, σ_m mean stress, σ_t tensile strength and σ_e alternative fatigue strength at stress ratio $R = -1$. The modified Goodman line agreed well with the results of the present fatigue test. The design methodology proposed for the metal fatigue is applicable to the sintered Si_3N_4 examined in this study.

To clarify the effects of volume on cyclic fatigue at room temperature, cyclic fatigue tests under alternative load were carried out, using two kinds of specimens with different volumes. Figure 3 shows the results of cyclic fatigue tests at room temperature, in which tensile specimens and cantilever beam specimens of SSN-B were used. Fatigue strength at the same number of cycles decreased with increasing effective volume. However, the slope of the S-N curve of the cantilever beam specimens, which have a small effective volume, is larger than that of tensile specimens, which have a large volume. The threshold stress of cyclic fatigue may be obtained by extrapolating for the point at which two curves intersect.

3 Cyclic Fatigue Behavior at High Temperature

Fatigue data for sintered Si_3N_4 (SSN-A3) with a glassy grain boundary phase at 800, 1000°C and room temperature were plotted in a log-log plot of stress versus number of cycles to failure, as shown in Fig. 4.⁸ The mean tensile strengths of 6-mm diameter

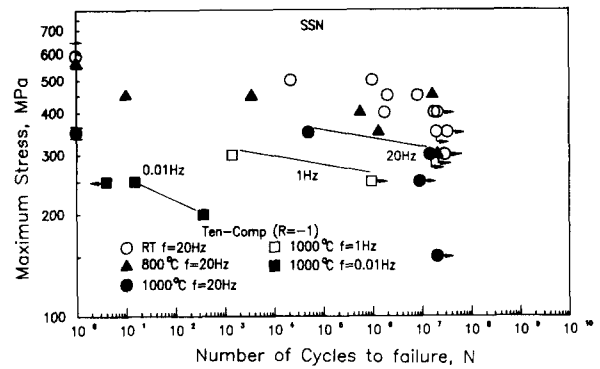


Fig. 4. S-N diagram of SSN-A3 using axial tension-compression load control at room temperature, 800 and 1000°C. The symbols on the vertical axis represent the tensile strength of the materials used.

button-head specimens at room temperature, 800 and 1000°C were 585, 560 and 360 MPa, respectively. The arrow pointing to the left indicates the specimen fractured at the onset of loading, and the ones pointing to the right indicate that the tests were suspended at that cycle without failure of the specimen. There was a large scatter, but the fatigue life of the specimens greatly increased as stress amplitude decreased.

At room temperature, fatigue strength at 10^7 cycles was about 60% of the original strength. Cyclic fatigue degradation at 1000°C with a stress ratio of -1 at a frequency of 20 Hz was smaller than at room temperature. In contrast to cyclic fatigue behavior at room temperature, the onset of fatigue life at 1000°C depended on frequency, as shown in Fig. 4. For a given high temperature, the lower the frequency, the less the fatigue resistance. Low cycle fatigue at high temperatures would be dominated by time-dependent fatigue.

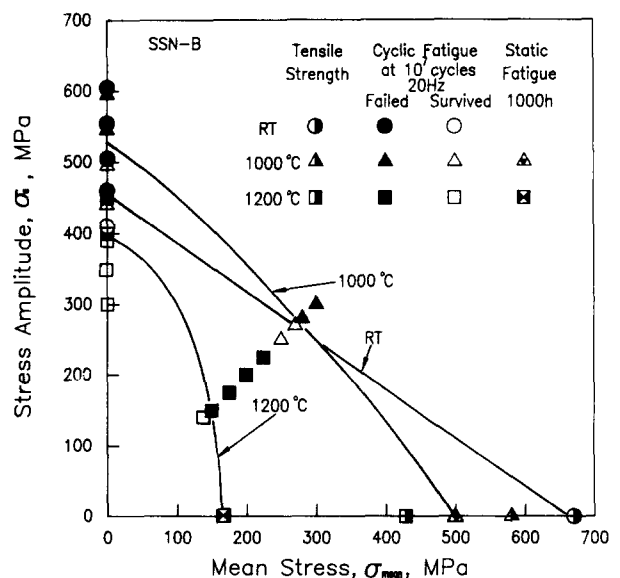


Fig. 5. Tensile mean stress effects on cyclic fatigue of SSN-B at room temperature, 1000 and 1200°C.

Cyclic fatigue behavior and life predictions are much more complicated at high temperature than at room temperature. Factors such as frequency, wave shape and creep, which have little consequence at room temperature, become important at high temperature.

The effects of mean tensile stress and static fatigue on cyclic fatigue of sintered Si_3N_4 (SSN-B) with a crystalline grain boundary phase at high tempera-

ture are shown in Fig. 5. These results were obtained under load control at a constant frequency of 20 Hz. The vertical axis represents a fully reversed fatigue condition and the horizontal axis represents static fatigue strength and ultimate tensile strength. As temperature increased, static fatigue strength decreased. The boundary within which the safety stress region is present tends to become elliptical as the temperature increases. An approximation for mean

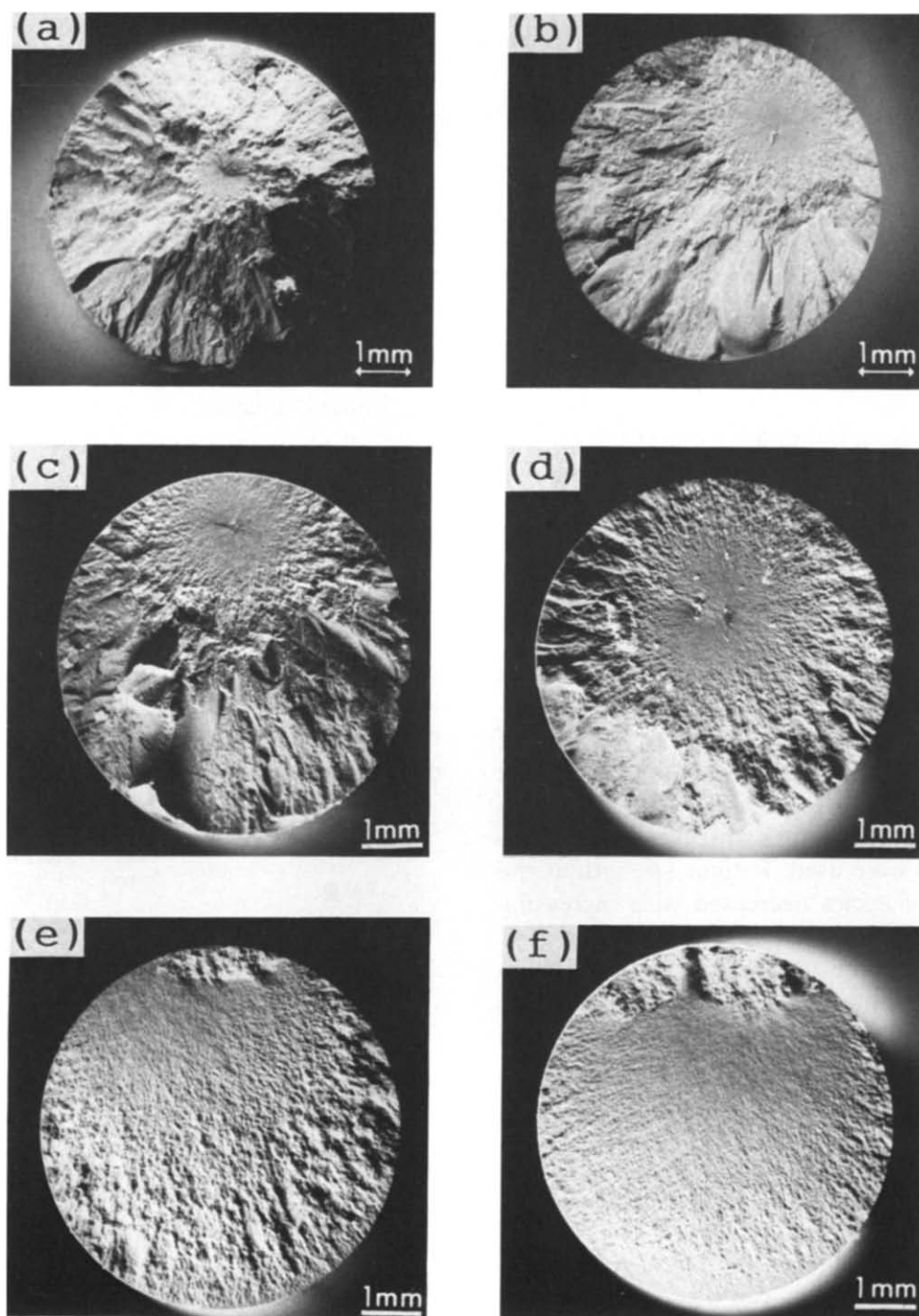


Fig. 6. Typical fracture surfaces of fatigue specimens of SSN-A3. (a) RT, 20 Hz, ± 500 MPa, 2.2×10^4 cycles; (b) RT, 20 Hz, ± 400 MPa, 1.8×10^7 cycles; (c) 800°C, 20 Hz, ± 350 MPa, 1.3×10^6 cycles; (d) 1000°C, 20 Hz, ± 350 MPa, 5.0×10^4 cycles; (e) 1000°C, 1×10^2 Hz, ± 200 MPa, 3.7×10^2 cycles; (f) 1000°C, 150 MPa, 204 h.

stress effect is shown in eqn (2) for high temperatures,⁹

$$\left(\frac{\sigma_a}{\sigma_e}\right)^n + \left(\frac{\sigma_m}{\sigma_s}\right)^n = 1 \quad (2)$$

where σ_a is stress amplitude, σ_m mean stress, σ_e alternating fatigue strength and σ_s static fatigue strength. The n value increased with increasing temperature.

4 Cyclic Fatigue Mechanism

The fractured surfaces of several specimens of SSN-A3 were examined through an optical microscope in order to determine fracture origins and failure modes. Major defects such as pores and inclusions are preferential nucleation and crack propagation sites, as shown in Fig. 6.¹⁰ In the case of the specimen fractured at room temperature, mirror and mist areas were clearly observed on the fracture surfaces, and the size of the mirror areas were correlated with stress amplitude and the number of cycles to failure. Microcracks at grain boundaries were observed in specimens that failed under cyclic load, as shown in Fig. 7.

At room temperature, alternating load accelerates fatigue faster than pulsating load. A mirror surface is found around the fracture origin in such cases as instantaneous and static fatigue fracture, as shown in Fig. 6. In the microstructure of specimens that fractured under cyclic stress at room temperature, clusters of microcracks were found sporadically at grain boundaries, as shown in Fig. 7. Some microcracks extended to join other microcracks, breaking elongated Si_3N_4 grains. From the above experimental results, cyclic fatigue mechanisms possibly involve a crack nucleation model and crack propagation model.

The crack nucleation model of a fatigue mechanism is as follows: a microcrack is caused by stress concentration around an initial flaw or heterogeneous portion in the microstructure. The microcracks and the initial flaw form a fatigue damage zone. If the fatigue damage zone grows too large or the crack density within it reaches a critical value, a cyclic fatigue failure occurs.

The crack propagation model of a fatigue mechanism is as follows: a microcrack is caused by stress concentration at the tip of an initial flaw. The microcracks emanate from the initial flaw. Cyclic fatigue failure occurs as the initial flaw grows to its critical size during testing. Crack propagation is faster under cyclic load than under static load.

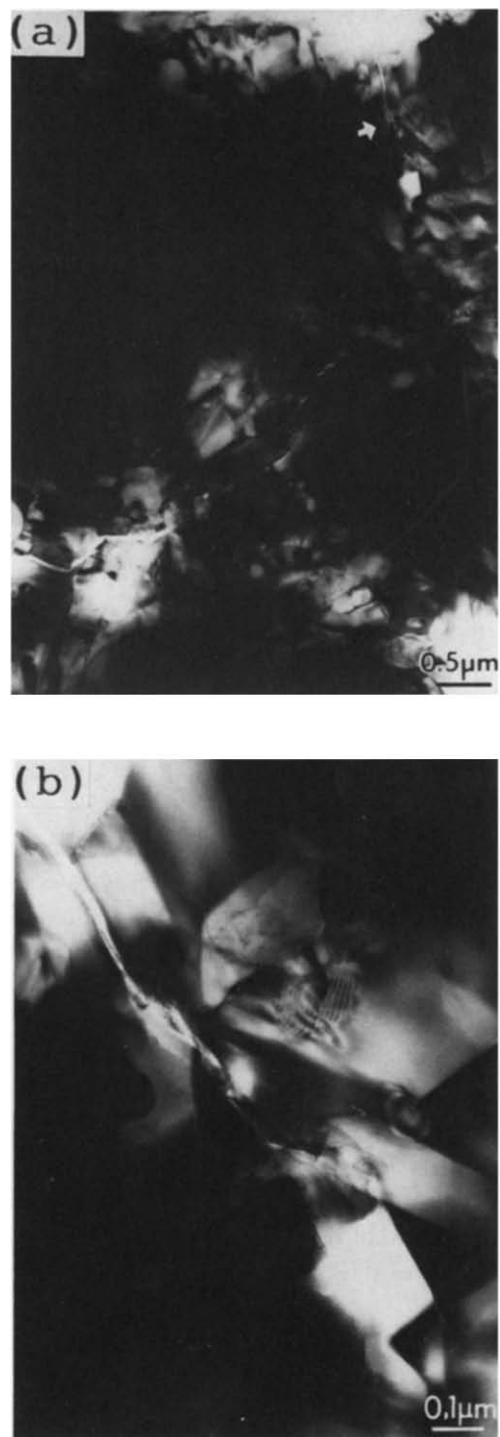


Fig. 7. Typical microstructures of SSN-A3 after fatigue test at room temperature. (a) ± 450 MPa, 8.2×10^6 cycles; (b) enlarged view of area marked with arrow in (a).

In the case of high cyclic fatigue of sintered Si_3N_4 (SSN-A3) with a glassy grain boundary phase at 800 and 1000°C, major defects such as pores and inclusions are preferential nucleation and crack propagation sites, as shown in Fig. 6(c) and (d), likely at room temperature, as shown in Fig. 6(a) and (b). However, slow crack regions were clearly observed around major defects. No major defect as fracture

origin was observed in the fracture surface of low cyclic fatigue specimen, as shown in Fig. 6(e). The surface had the creep deformation region in such cases as static fatigue fracture surface, as shown in Fig. 6(f).

5 Conclusions

- (1) Degradation in the strength of sintered Si_3N_4 by cyclic fatigue at room temperature depended mainly on the number of cycles rather than on time.
- (2) The cyclic fatigue life of sintered Si_3N_4 at high temperatures depended on frequency. The lower the frequency, the less the resistance to fatigue.
- (3) A failure diagram was constructed to show the effects of mean stress and stress amplitude on fatigue strength. An equation expressing the allowable stress under cyclic loading was proposed.
- (4) Microstructural observations suggest that the cyclic fatigue of sintered Si_3N_4 progressed by the formation of microcracks at grain boundaries. The progress of cyclic fatigue at high temperatures is caused by slow crack growth and creep deformation.

Acknowledgment

A part of this work was conducted under a contract between the Agency of Industrial Science and Technology of the Ministry of International Trade and Industry (MITI) and the Engineering Research Association for High Performance Ceramics as a

part of the R&D Project of Basic Technology for Future Industries.

References

1. Boyd, G. L. & Kreiner, D. M., AGT 101/ATTAP ceramic technology development. In *Proceedings of the Twenty-Fifth Automotive Technology Development Contractors' Coordination Meeting*, 26–29 October 1987, pp. 101–14.
2. Kobayashi, Y., Miyauchi, J., Matsuo, E. & Inagaki, T., Hot gas spin testing of ceramic radial turbine rotors. In *Proceedings of the 1987 Tokyo International Gas Turbine Congress*, 26–31 October 1987, pp. I177–81.
3. Tsukawaki, Y., Shimano, K., Shigetsu, M., Takatou, M., Ogawa, Y. & Ogasawara, T., Development of all-ceramic swirl chamber of indirect engines—material engineering. In *Passenger Car Meeting & Exposition*, Dearborn, Michigan, 22–25 September 1986, SAE 861408.
4. Glover, D., A ball-rod rolling contact fatigue tester. In *Rolling Contact Fatigue Testing of Bearing Steels*, ed. J. J. C. Hoo. American Society for Testing and Materials, Philadelphia, PA, 1981, ASTM STP 771, pp. 107–24.
5. Masuda, M., Yamada, N., Soma, T., Matsui, M. & Oda, I., Fatigue of ceramics (Part 2)—cyclic fatigue properties of sintered Si_3N_4 at room temperature. *Nippon Seramikkusu Kyokai Gakuyutu Ronbunshi*, **97**(5) (1989) 520–4.
6. Masuda, M., Soma, T., Matsui, M. & Oda, I., Fatigue of ceramics (Part 1)—fatigue behavior of sintered Si_3N_4 under tension-compression cyclic stress. *Nippon Seramikkusu Kyokai Gakuyutu Ronbunshi*, **96**(3) (1988) 277–83.
7. Goodman, J., *Mechanics Applied to Engineering*. Longmans, Green & Co., London, 1899.
8. Masuda, M., Soma, T., Matsui, M. & Oda, I., Cyclic fatigue of sintered silicon nitride. In *Proceedings of the MRS International Meeting on Advance Materials*, 30 May–3 June Vol. 5, 1989, pp. 537–42.
9. Fuchs, H. O. & Stephens, R. I., *Metal Fatigue in Engineering*. John Wiley & Sons, New York, 1980.
10. Masuda, M., Soma, T., Matsui, M. & Oda, I., Fatigue of ceramics (Part 3)—cyclic fatigue behavior of sintered Si_3N_4 at high temperature. *Nippon Seramikkusu Kyokai Gakuyutu Ronbunshi*, **97**(6) (1989) 612–18.
11. Japanese Industrial Standard, Testing method for flexural strength (modulus of rupture) of high performance ceramics. JIS R1601, 1981.